Supporting Information

Trap-Free Halogen Photoelimination from Mononuclear Ni(III) Complexes

Seung Jun Hwang,[a] David C. Powers,[a] Andrew G. Maher,[a] Bryce L Anderson,[a] Ryan G. Hadt,[a] Shao-Liang Zheng,[a] Yu-Sheng Chen,[b] and Daniel G. Nocera[a,*]

[a]*Department of Chemistry and Chemical Biology, Harvard University, 12 Oxford Street, Cambridge, MA 02138–2902*

[b]*ChemMatCARS, The University of Chicago, Argonne, IL 60439*

Email: dnocera@fas.harvard.edu

Table of Contents ..... *Page*

A. Methods

Materials and Methods. NMR spectra were recorded at the Harvard University Department of Chemistry and Chemical Biology NMR facility on a Varian Unity/Inova 600 spectrometer operating at 600 MHz for ^{1}H acquisitions or a Varian Mercury 400 spectrometer operating at 160 MHz for ^{31}P acquisitions. NMR chemical shifts are reported in ppm with the residual solvent resonance used as an internal standard. ^{31}P NMR chemical shifts were referenced to an external 85% H_3PO_4 standard. EPR spectra were recorded on a Bruker ELEXIS E-580 spectrometer equipped with a Bruker ER4122 SHQE-W1 resonator and an Oxford Instruments ESR 900 cryostat. EPR spectra were simulated using EasySpin.[1] UV-vis spectra were recorded at 293 K in quartz cuvettes on a Spectral Instruments 400 series diode array and were blanked against the appropriate solvent. Solution magnetic moments were determined using the Evans method in CH_3CN and measured using ^{19}F NMR (hexafluoro-benzene added); diamagnetic corrections were estimated from Pascal constants.[2] Steady-state photochemical reactions were performed using a 1000 W high-pressure Hg/Xe arc lamp (Oriel) and the beam was passed through a water-jacketed filter holder containing the appropriate long-pass filter, an iris, and a collimating lens. $NiCl_2$(dme) (dme = 1,2-dimethoxyethane), $NiBr_2$(dme), dppey (dppey = *cis*-bis(diphenylphosphino)ethylene), and $NiCl_2$(dppe) (dppe = bis(diphenylphosphino)ethane) were obtained from Strem Chemicals. Bromine and dppe were obtained from Sigma Aldrich. $PhICl_2$ and $NiCl_2$(MeO-dppe) (MeO-dppe = 1,2-*bis*(di-4-methoxyphenyl)phosphino}ethane) were prepared according to reported procedures.[3,4] Ni(II) complexes containing bidentate phosphine ligands were prepared by treatment of NiX_2(dme) (X = Cl, Br) with an equimolar amount of the appropriate phosphine in THF.[5,6] Ni(III) trihalide complex **1a**, **1b** and **1c** were prepared by treating corresponding Ni(II) dihalide **2a**, **2b** and **2c** with 0.5 equiv of $PhICl_2$ or Br_2 as previously described.[7]

X-ray Crystallography. Structures and variable-temperature (VT) X-ray data were collected on a Bruker three-circle platform goniometer equipped with an Apex II CCD and an Oxford cryostream cooling device at 100 - 275 K. Radiation was supplied from either a graphite fine focus sealed tube Mo Kα (0.71073 Å) source. Crystals were mounted on a glass fiber using Paratone N oil. Data were collected as a series of φ and/or ω scans. Data were integrated using SAINT and scaled with either a numerical or multi-scan absorption

---

1 Stoll, S.; Schweiger, A. *J. Magn. Reson.* **2006**, *178*, 42.

2 Bain, G. A.; Berry, J. F. *J. Chem. Ed.* **2008**, *85*, 532.

3 Zielinska, A.; Skulski, L. *Tetrahedron Lett.* **2004**, *45*, 1087.

4 Fawcett, J.; Hope, E. G.; Stuart, A. M.; Sherrington, J. *Inorg. Chim. Acta.* **2006**, *359*, 3535.

5 Booth, G.; Chatt, J. *J. Chem. Soc.* **1965**, 3238.

6 McAuliffe, C. A.; Meek, D. W. *Inorg. Chem.* **1969**, *8*, 904.

7 Gray, L. R.; Higgins, S. J.; Levason, W.; Webster, M. *J. Chem. Soc. Dalton Trans.* **1984**, 459.

correction using SADABS. The structures were solved by intrinsic phasing using SHELXT (Apex2 program suite v2014.1) and refined against F^2 on all data by full matrix least squares with SHELXL-97. All non-hydrogen atoms were refined anisotropically. Hydrogen atoms were placed at idealized positions and refined using a riding model.

Photocrystallography data was collected using 0.41328 Å radiation at 15 K (Oxford Diffraction Helijet) on a vertically mounted Bruker D8 three-circle platform goniometer equipped with an Apex II CCD at ChemMatCARS located at the Advanced Photon Source, Argonne National Laboratory. Illumination was provided by a Thorlabs 365 nm LED (M365L2) and was delivered to the sample via a 100 μm (i.d.) fiber optic. Dark structures were solved and refined as described above. For data sets obtained during irradiation, non-H atoms of the product were located in difference Fourier maps, calculated with coefficients F_0(irradiated) − F_0(dark), and then refined with constraints on the product molecule's atomic displacement parameters to the corresponding values of the reactant molecule (EADP instructions of SHELXL97). The percentage of the reactant in the crystal was treated as a variable in the refinements.

Halogen Quantification. The yield of evolved Cl_2 and Br_2 were quantified colorimetrically by trapping evolved halogen with *N,N*-diethyl-1,4-phenylenediamine sulfate (DPD) to afford the pink radical cation $DPD^{\bullet+}$. Formation of $DPD^{\bullet+}$ was monitored by UV-vis spectroscopy and quantified against a standard curve obtained by addition of known amount of bromine to 5 mM DPD solution in water. As displayed in Fig S11, $DPD^{\bullet+}$ radical formation is linearly correlated to the concentration of bromine employed. When DPD was the limiting reagent in oxidation reaction, the amount of $DPD^{\bullet+}$ radical generated was the same for either Br_2 or Cl_2 as the oxidant. Evolved halogen from solid-state photolysis was obtained from the same standard concentration curve.

A representative procedure for determining halogen photoevolution yields is as follows: Films of complex **1a** (5 mg) were deposited on the wall of one of the chambers in "H" cell reactor by evaporation. 5 mM DPD solution in water was then placed in another chamber and the solution was frozen to 77 K while the entire reaction vessel was evacuated. After 12 h of irradiation, the two sides of the reactor were separated by closing a Teflon stopcock and thawing the frozen DPD solution. When vacuum transferred halogens were completely dissolved in DPD solution, the UV-vis spectrum was taken to calculate the amounts of halogen evolved from photolysis.

Quantum Yield Measurements. Quantum yields for conversion of complexes **1** to **2** were determined by chemical actinometry against a potassium ferrioxalate standard.[8] In

[8] Montalti, M.; Credi, A.; Prodi, L.; Gandolfi, M. T. *Handbook of Photochemistry*, 3rd ed.; Taylor and Francis: Boca Raton, 2006.

addition to band pass filters, an additional filter (Hg line, 370 nm, 434 nm or 510 nm) was employed to generate a monochromatic beam. Average photon flux was determined from the average of actinometry performed before and after measurements on **1**. For 370 nm measurements, a 0.006 M ferrioxalate solution was used. Because of the small absorbance of the actinometer at 434 nm and 510 nm, the concentration of complex was increased to 0.15 M for measurements at these wavelengths. The photoreaction from **1** to **2** proceeded cleanly, thus allowing the number of moles of **2** formed to be calculated.

Solid-State Photolysis. Solid-state photolysis experiments were carried out in a two-chamber "H" reactor that was custom made by James Glass of Hanover, MA. The two chambers could be isolated from each other with a Teflon stopcock. Films of **1** were deposited on the wall of one of the chambers by evaporation; samples of 10 to 40 mg were deposited from solutions in CH_2Cl_2. The reaction vessel was evacuated and the sample was then irradiated using a 350 nm long-pass filter; the other side of the reaction vessel was cooled to 77 K during irradiation. The reactor was periodically rotated so as to present unphotolyzed **1a** to the incident light. After 10 h of irradiation, the two sides of the cell were separated by closing the Teflon stopcock. Unreacted **1a** was recovered in 45% yield based on the UV-vis spectrum.

The liquid nitrogen cooled compartment of the H-cell described above was connected to He carrier gas and an in-line mass spectrometer (Agilent Technologies 5975C Mass Selective Detector) and purged for 2 h before data collection. The mass spectrometer was operated in selective ion mode that monitored for 35 (Cl_2 fragment), 37 (Cl_2 fragment), 70 (Cl_2), 72 (Cl_2), 74 (Cl_2), and 44 (CO_2) amu. After a stable baseline was reached, the frozen compartment was rapidly warmed by immersion in water while MS data was collected in real-time. Data were collected until all gas levels returned to their baseline values. The percent abundance for 35 and 37 ions were computed using the following equations: $^{35}Cl = [2 \times {}^{35}Cl + {}^{72}Cl + 2 \times {}^{70}Cl]/[2 \times ({}^{35}Cl + {}^{37}Cl + {}^{70}Cl + {}^{72}Cl + {}^{74}Cl)]$; $^{37}Cl = [2 \times {}^{37}Cl + {}^{72}Cl + 2 \times {}^{74}Cl]/[2 \times ({}^{35}Cl + {}^{37}Cl + {}^{70}Cl + {}^{72}Cl + {}^{74}Cl)]$ (^{n}Cl = counts at n amu).

Time-Resolved Photochemistry. Nanosecond resolved transient absorption (TA) spectroscopy experiments were performed using a system described previously,[9] but with an iHR320 spectrometer. The 355 nm laser pulses (8 - 10 ns at FWHM) used for excitation were generated using the third harmonic of a 10 Hz Nd:YAG pulsed laser. The white-light continuum was provided by a Xe-arc lamp set to 2.0 ms pulses with 30 A current. A 500-nm blazed grating (300 grooves/mm) was used for all experiments. For full spectrum TA acquisitions, the entrance slit was set to 0.16 mm (2.0 nm resolution) and the gate time for the CCD was 60 ns. For single-wavelength kinetics experiments, the entrance and exit slits were set to 0.06 mm (0.75 nm resolution), and 1.0 kV bias was used for the PMT. The full

[9] Holder, P. G.; Pizano, A. A.; Anderson, B. L.; Stubbe , J.; Nocera, D. G. *J. Am. Chem. Soc*. **2012**, *134*, 1172.

spectra are averages of 50 - 100 four-spectrum sequences and the single-wavelength kinetics traces are averages of 1000 acquisitions. Sample solutions were prepared in an N_2-atmosphere glovebox using glass scintillation vials sealed with rubber septa. During TA acquisitions, solutions were flowed without recirculation through a 3-mm diameter, 1-cm path length flow cell (Starna, type 585.2) using a peristaltic pump and positive N_2 pressure.

B. Structural Data for $NiBr_3$(dppe) (1b)

Table S1. X-ray experimental details for complex **1b** (CCDC 1040258)

Crystal Data	
Chemical formula	$C_{27}H_{26}Br_3Cl_2NiP_2$
Fw, g/mol	781.76
Crystal system, space group	Monoclinic, *P2(1)/n*
Temperature (K)	100(2)
a, *b*, *c* (Å)	13.5432(7), 15.0186(8), 14.8428(7)
α, β, γ (°)	90, 111.8000(8), 90
V (Å^3)	2803.1(2)
Z	4
Radiation type	Mo *K*α
μ (mm^{-1})	5.290
Crystal size (mm)	0.12 × 0.07 × 0.03
Data collection	
Diffractometer	Bruker *APEX*-II CCD
Absorption correction	Multi-scan, *SADABS*
T_{min}, T_{max}	0.5670, 0.8617
No. of measured, independent and observed [$I > 2\sigma(I)$] reflections	25749, 4944, 3766
R_{int}	0.0668
$(\sin \theta/\lambda)_{max}$ (Å^{-1})	0.610
Refinement	
$R[F^2 > 2\sigma(F^2)]$, $wR(F^2)$, S	0.0433, 0.1086, 1.038
No. of reflections	4944
No. of parameters	316
No. of restraints	0
H-atom treatment	H atoms treated by a mixture of independent and constrained refinement
Dr_{max}, Dr_{min} (e Å^{-3})	1.112, –1.577

C. EPR Spectroscopy

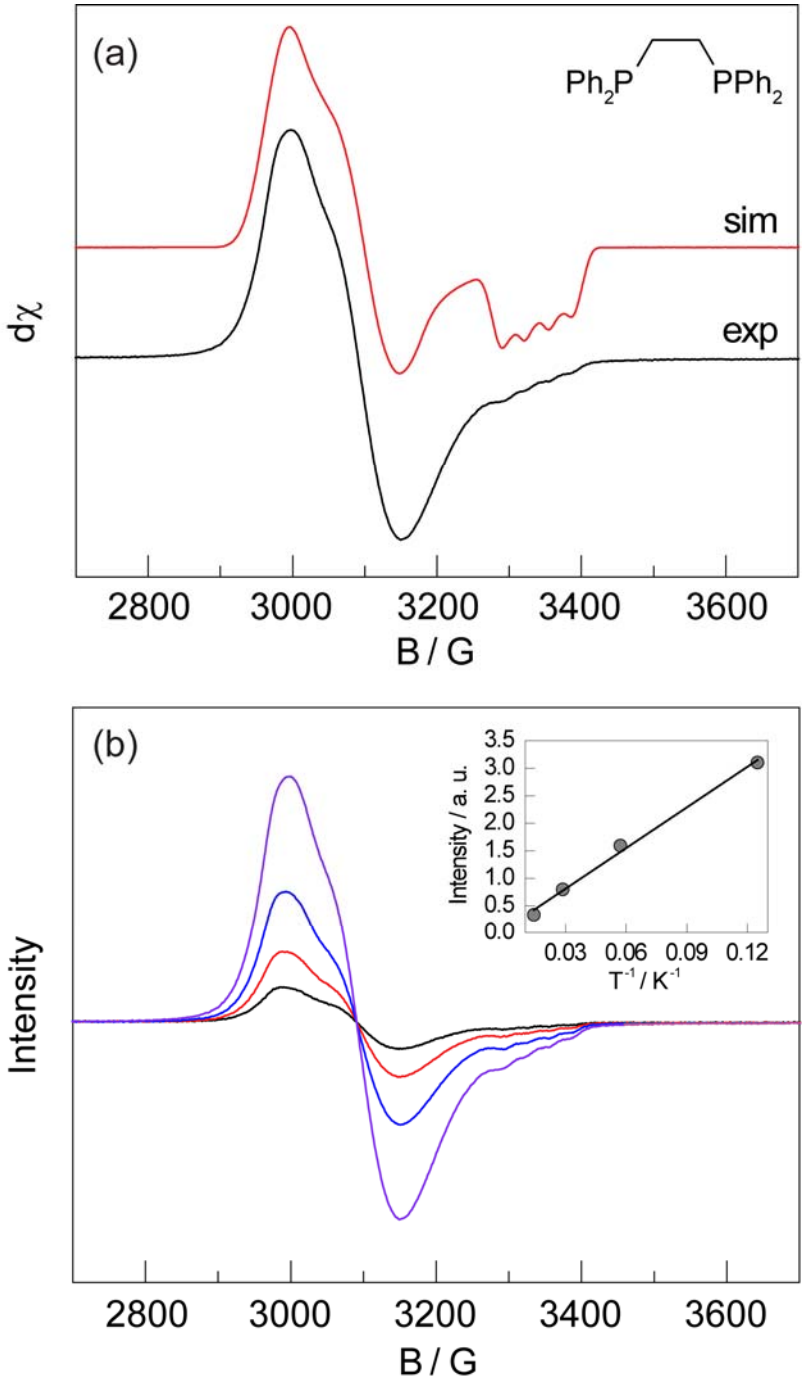

Figure S1. (a) EPR spectrum of complex **1a** recorded at 8 K in 1:1 CH_3CN/toluene solution (—, black) and simulated (—, red). (b) EPR spectrum of frozen solution of **1a** in 1:1 CH_3CN/toluene obtained at 70.0 K (—, black) 35.0 K (—, red), 17.5 K (—, blue), and 8.0 K (—, purple). Inset: plot of intensity at 2997 G versus temperature.

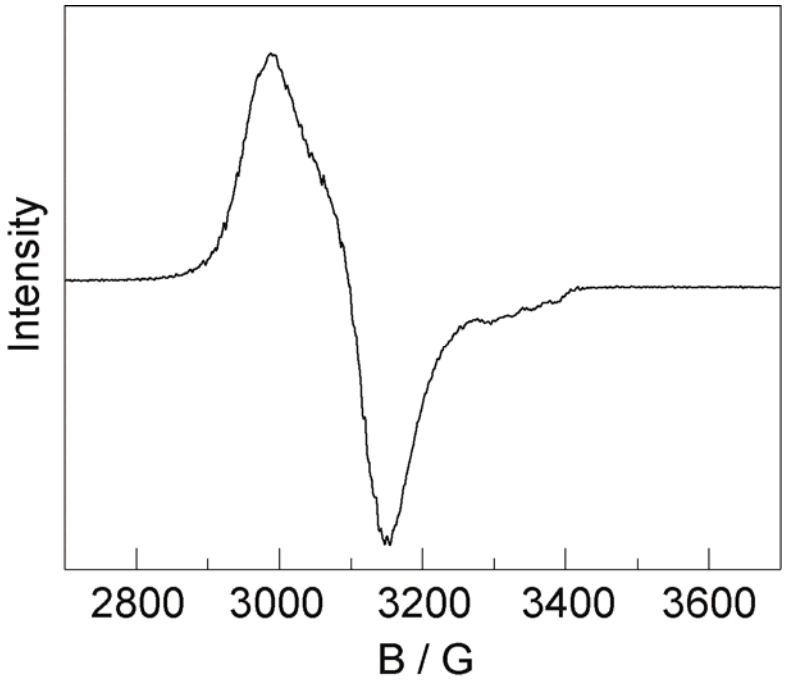

Figure S2. EPR spectrum of complex **4-MeO-1a** recorded at 77 K in 1:1 CH_3CN/toluene solution.

D. Steady-State Photolysis Experiments

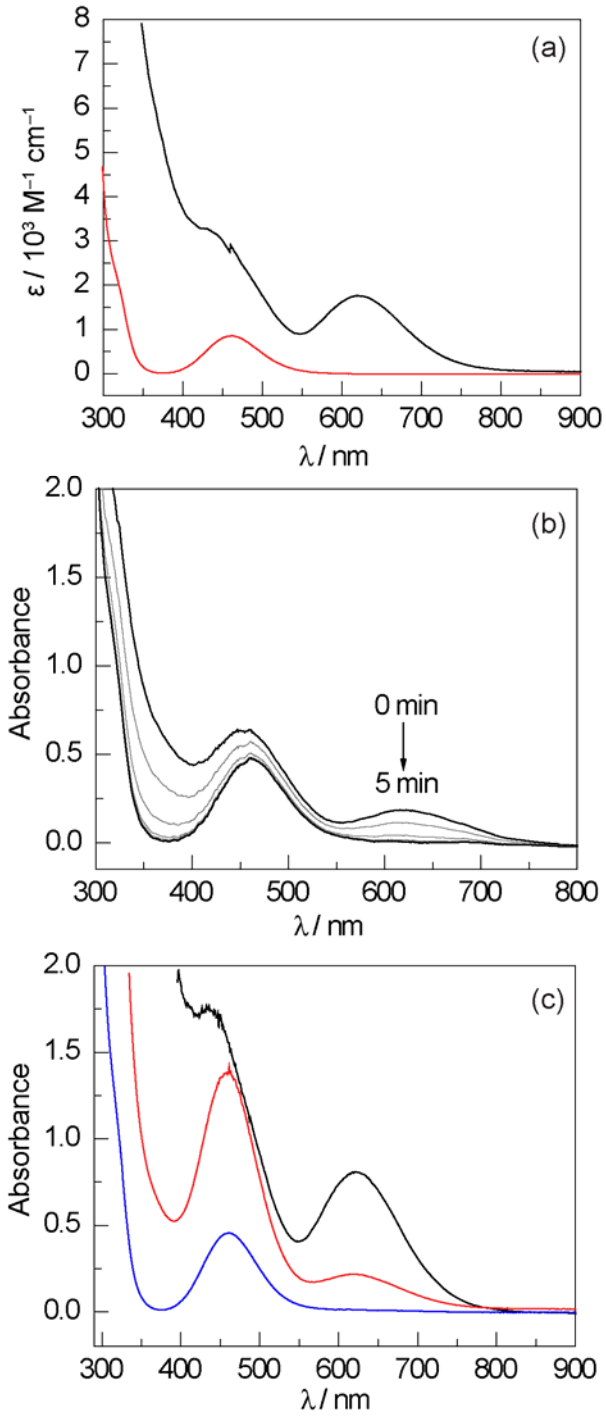

Figure S3. (a) Extinction spectra of complexes **1a** (—, black) and **2a** (—, red). (b) Spectral evolution for the photolysis of 0.2 mM of complex **1a** in MeCN (λ_{exc} > 400 nm). (c) Electronic absorption spectra of Ni complex **1a** in MeCN (—, black), the solid-state photolysis product in MeCN after 9 h (—, red), and 18 h (—, blue) of irradiation (λ > 350 nm).

E. NMR data

Though Ni(II) complexes **2a**, **2b**, and **2c** were previously reported,[5,6] the NMR data for these complexes has not been reported. The measured NMR data are tabulated below. The corresponding Ni(III) complexes are silent in both ^{1}H and ^{31}P NMR.

$NiCl_2$(dppe) (**2a**): ^{1}H NMR (600 MHz, CD_3CN) δ (ppm): 7.99 (m, 8H), 7.63 (m, 4H), 7.55 (m, 8H), 2.21 (m, 4H); ^{31}P NMR (160 MHz, CD_3CN) δ (ppm): 59.8.

$NiBr_2$(dppe) (**2b**): ^{1}H NMR (600 MHz, CD_2Cl_2) δ (ppm): 7.98 (m, 6H), 7.61 (m, 3H), 7.54 (m, 6H), 2.09 (m, 4H); ^{31}P NMR (160 MHz, CD_2Cl_2) δ (ppm): 66.3.

$NiBr_2$(dppey) (**2c**): ^{1}H NMR (600 MHz, CD_2Cl_2) δ (ppm): 7.90 (m, 8H), 7.60 (m, 3H), 7.52 (m, 4H), 6.83 (dd, 2H); ^{31}P NMR (160 MHz, CD_2Cl_2) δ (ppm): 73.6.

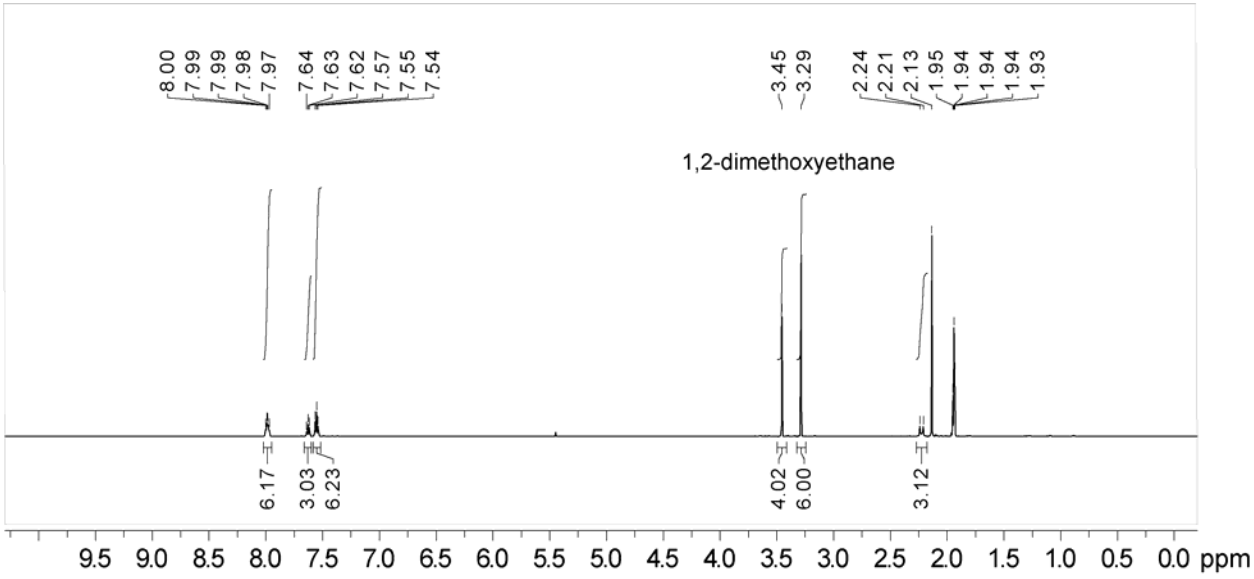

Figure S4. ^{1}H NMR spectrum of the reaction solution (12.4 mM) obtained by photolysis of **1a** with visible light (λ > 430 nm) recorded in CD_3CN at 23 °C. 1,2-Dimethoxyethane was added as an external standard.

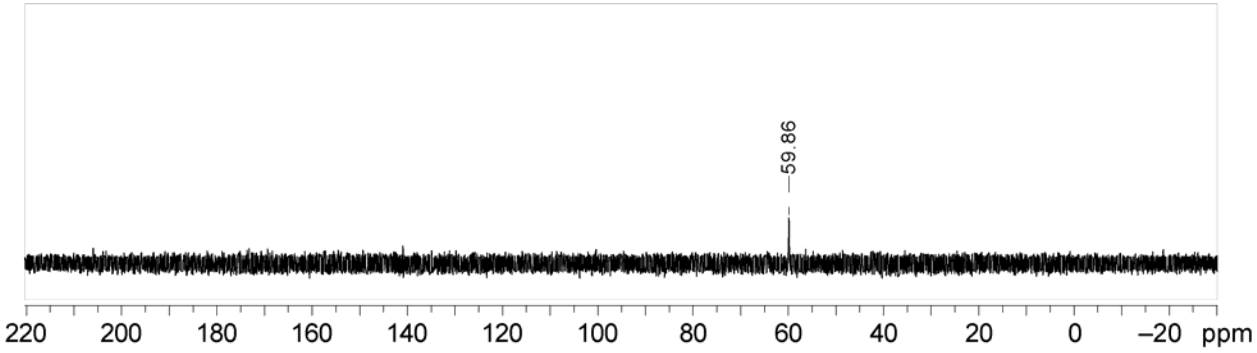

Figure S5. ^{31}P NMR spectrum of the reaction solution (12.4 mM) obtained by photolysis of **1a** with visible light (λ > 430 nm) recorded in CD_3CN at 23 °C.

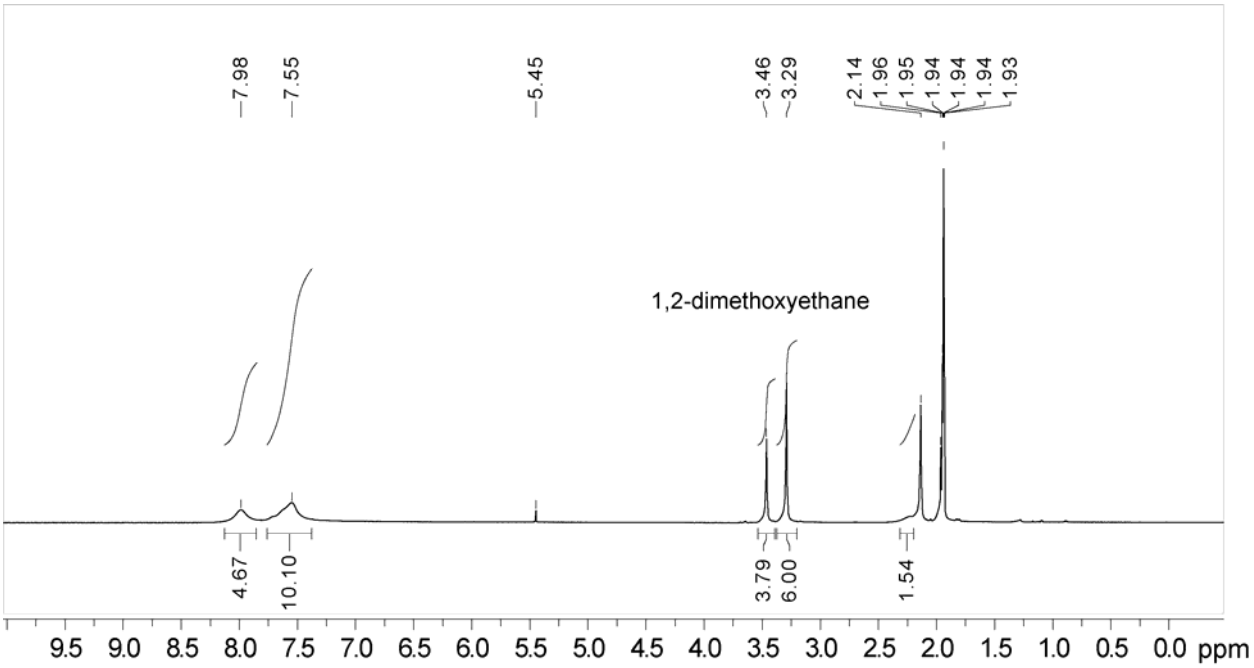

Figure S6. ^{1}H NMR spectrum of the photoproducts of solid-state photolysis of **1a** with visible light (λ > 350 nm) recorded in CD_3CN at 23 °C. 1,2-Dimethoxyethane was added as an external standard.

F. Halogen Quantification

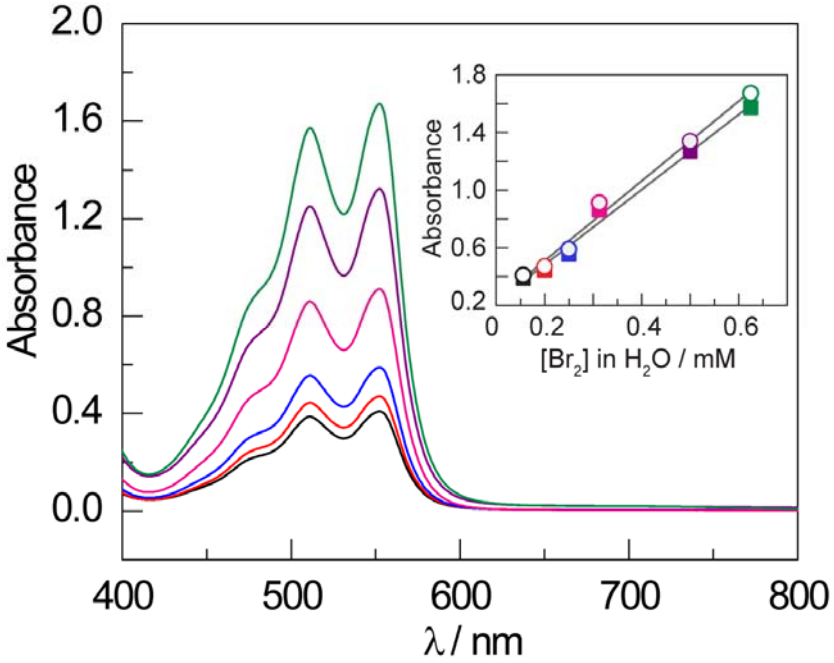

Figure S7. UV-vis absorption spectrum showing formation of $DPD^{\bullet+}$ when DPD is treated with different concentrations of Br_2 in H_2O. The spectrum was recorded at room temperature. Inset shows concentration dependent absorbance, λ_{max} at 552 nm (circles) and λ_{max} at 511 nm (squares).

G. Thermal Stability Test in Solid State

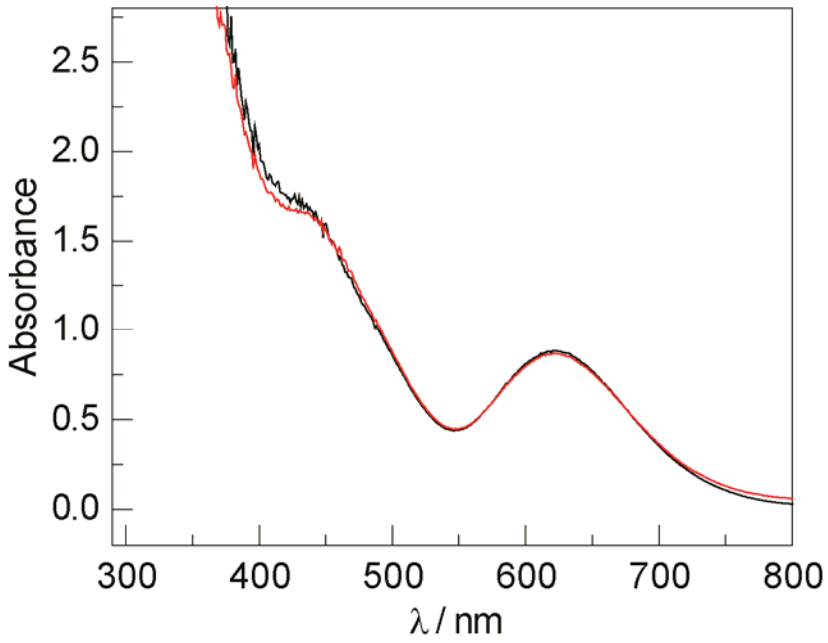

Figure S8. Electronic absorption spectra of complex **1a** in MeCN (—, black) and after heating at 70 °C for 2 d in solid state (—, red). Complex **1a** is water sensitive. Much more rapid thermal decomposition (resulting in the formations of Ni(II) complex **2a** is observed from **1a** when moisture is not rigorously excluded. In the exclusion of water, complex **1a** does decompose at 110 °C to generate Ni(II) complex **2a**. The moisture sensitivity of **1a** may account for previously suggested thermal instability of **1a** (Gray, L. R.; Higgins, S. J.; Levason, W.; Webster, M. *J. Chem. Soc. Dalton Trans*. **1984**, 459.)

H. Solution Calorimetry Measurements

Representative Procedure. In the glove box, a solution of 0.488 g (0.79 mmol) of $NiBr_2$(dppe) (**2b**) in 100 mL of anhydrous CH_2Cl_2 was prepared. This solution was transferred to a glass cell for the Thermometric 2225 Precision Solution Calorimeter, which was equipped with an ampoule-breaking rod. A small glass ampoule containing 0.031g Br_2 (0.194 mmol) was added, sealed, and loaded into the calorimeter. Following temperature equilibration (achieved standard deviation of 2 μK after 2 h), the reaction was initiated by breaking the ampoule and rotating the calorimeter to ensure complete mixing. Electrical calibrations were run before and after breaking the ampoule.

In the case of chloride Ni complexes, the enthalpy of interest was obtained based on the equations below.

(1) 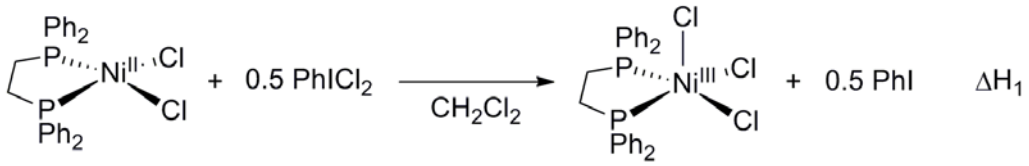

(2) 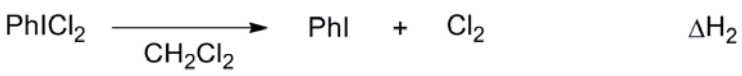

---

(3) 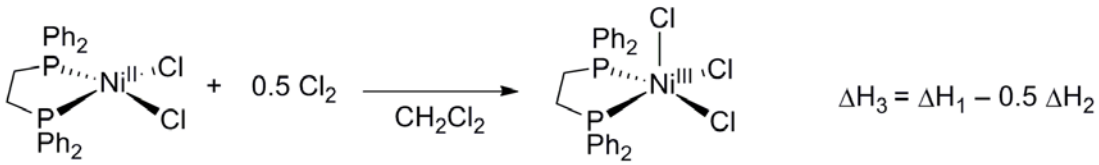

Measured data based on the reaction of the solid $PhICl_2$ was corrected for the enthalpy of solution of the solid $PhICl_2$, which was measured separately. The enthalpy of solution of iodobenzene and 0.194 M Br_2 in CH_2Cl_2 were also measured for the purposes of a solvation correction. Reported data is the average of three independent measurements.

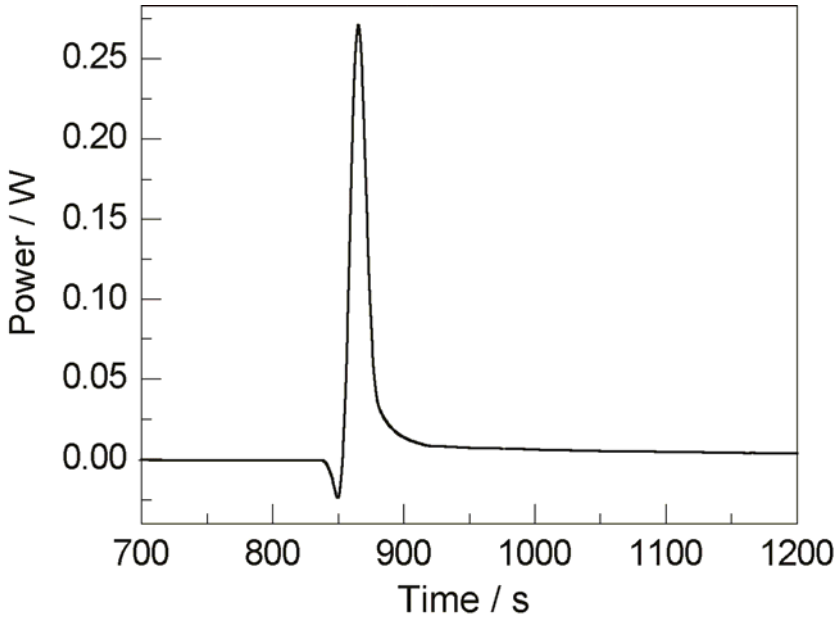

Figure S9. Thermogram for reaction of $NiCl_2$dppe (**2a**) and $PhICl_2$ in CH_2Cl_2.

I. Nanosecond Transient Absorption Spectroscopy

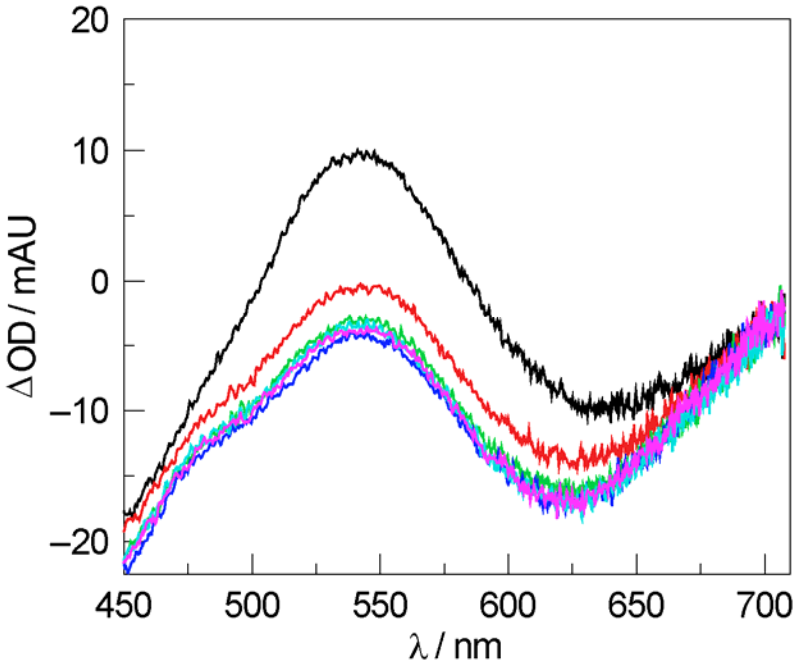

Figure S10. Transient absorption spectra obtained by laser flash photolysis of complex **1a** (355 nm pump) as a 0.44 mM solution in MeCN. Transient absorption spectra recorded 40 ns (black), 4 μs (red), 8 μs (green), 12 μs (blue), 16 μs (light blue), and 20 μs (pink) after the laser pulse.

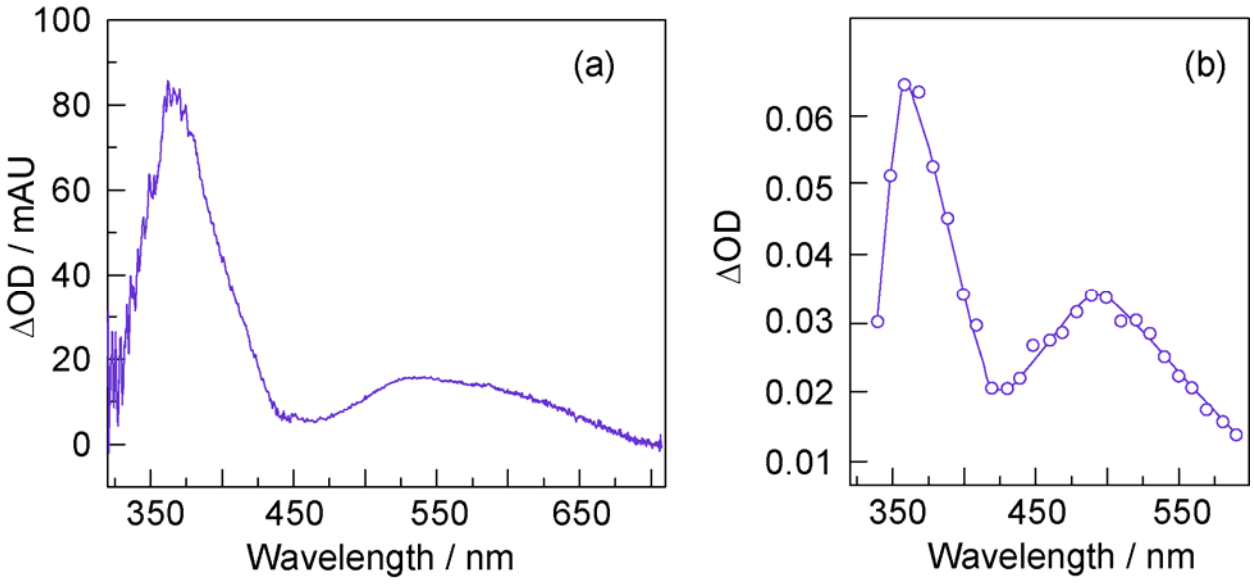

Figure S11. (a) Comparison between (a) transient absorption spectrum generated by subtracting the difference spectrum of a 0.44 mM solution of **1a** in CH_3CN acquired at a 50 μs time delay from that acquired at a 40 ns time delay (λ_{exc} = 355 nm) and (b) the chlorine-atom charge transfer adducts of benzene, generated by laser radiolysis (Data was adapted from reference 32 of text). Single wavelength kinetics were monitored at 540 nm and provided a lifetime of 3.43 ± 0.05 μs for intermediate **4**. For comparison, the lifetime of the charge-transfer complex of benzene and a chlorine radical is ~1 μs in acetonitrile and 3.9 μs in carbon tetrachloride (Refs: Förgeteg, S.; Bérces, T. *J. Photochem. Photobiol. A: Chem,* **1993**, *73,* 187; Bühler, R. E.; Ebert, M. *Nature*, **1967**, *214*, 1220.)

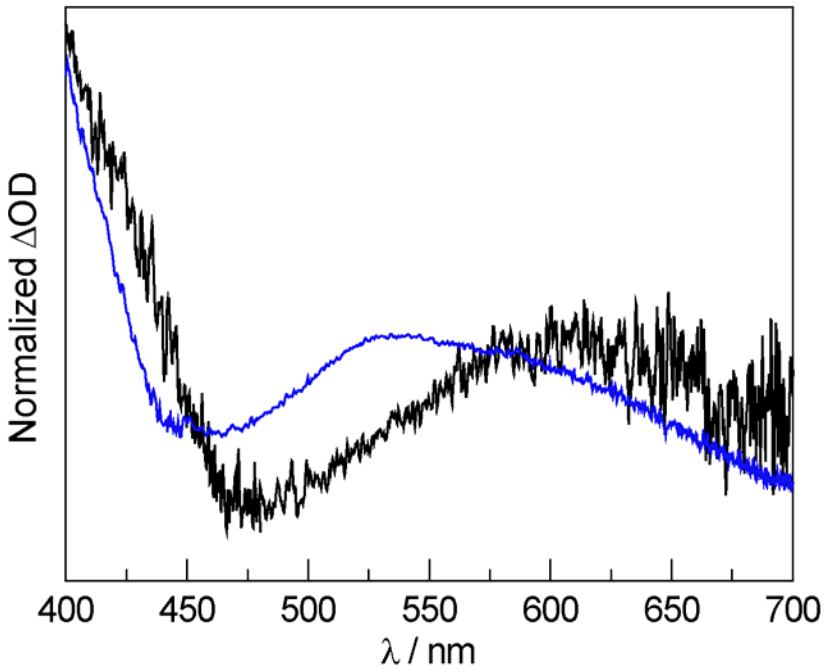

Figure S12. Transient absorption spectra pumped at 355 nm for **1a** (—, blue) and *para*-methoxy substituted **1a** (—, black). The spectrum was generated by subtracting the TA difference spectrum acquired at a 50 μs time delay from that acquired at a 40 ns time delay.

J. Photocrystallography Data Analysis

J.1. Structural Data of $NiBr_3$(dppey) (1c)

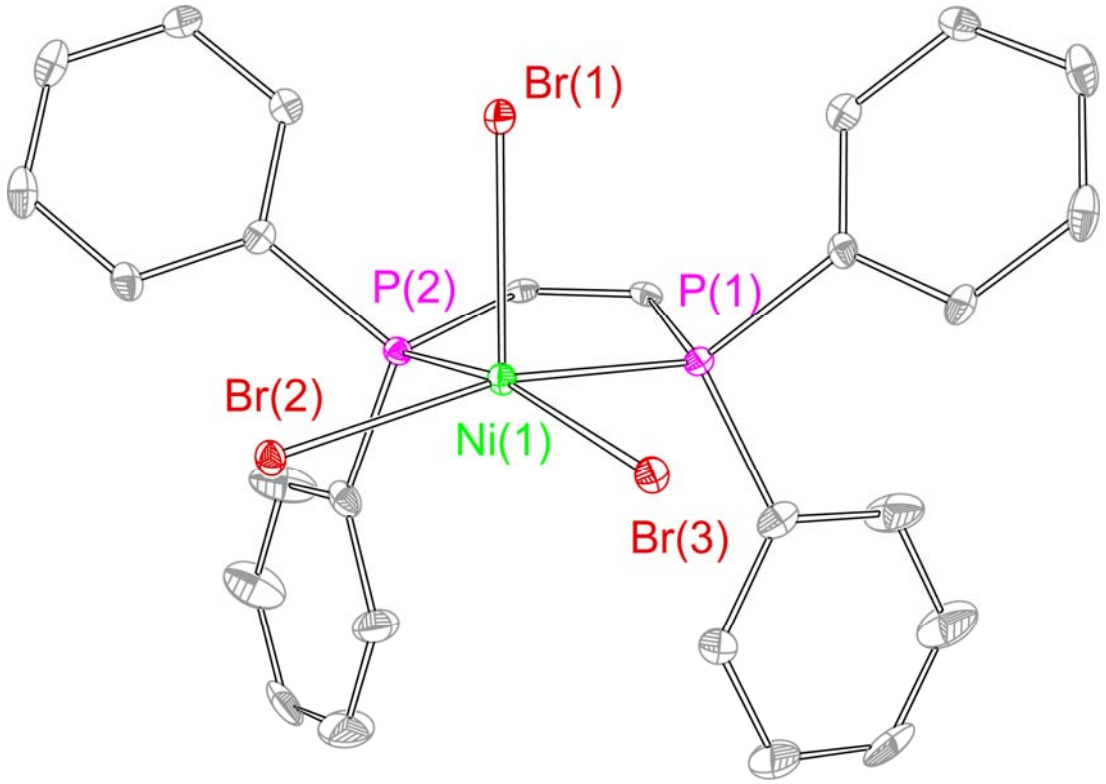

Figure S13. Thermal ellipsoid plot of $NiBr_3$(dppey) (**1c**) drawn at the 50% probability level. H-atoms omitted for clarity.

Table S2. X-ray experimental details for complex **1c** (CCDC 1040261)

Crystal Data	
Chemical formula	$C_{28}H_{26}Br_3Cl_4NiP_2$
Fw, g/mol	864.67
Crystal system, space group	Orthorhombic, *Pnma*
Temperature (K)	100(2)
a, *b*, *c* (Å)	23.482(1), 16.8828(7), 7.9874(4)
α, β, γ (°)	90, 90, 90
V (Å^3)	3166.6(2)
Z	4
Radiation type	Mo *K*α
μ (mm^{-1})	4.856
Crystal size (mm)	0.12 × 0.10 × 0.05
Data collection	
Diffractometer	Bruker *APEX*-II CCD
Absorption correction	Multi-scan, *SADABS*
T_{min}, T_{max}	0.5934, 0.7933
No. of measured, independent and observed [$I > 2\sigma(I)$] reflections	44712, 2909, 2330
R_{int}	0.0456
$(\sin \theta/\lambda)_{max}$ (Å^{-1})	0.610
Refinement	
$R[F^2 > 2\sigma(F^2)]$, $wR(F^2)$, S	0.0296, 0.0602, 1.025
No. of reflections	2909
No. of parameters	182
No. of restraints	1
H-atom treatment	H atoms treated by a mixture of independent and constrained refinement
Dr_{max}, Dr_{min} (e Å^{-3})	0.481, –0.709

J.2. Photocrystallography of $NiBr_3$(dppey) (1c)

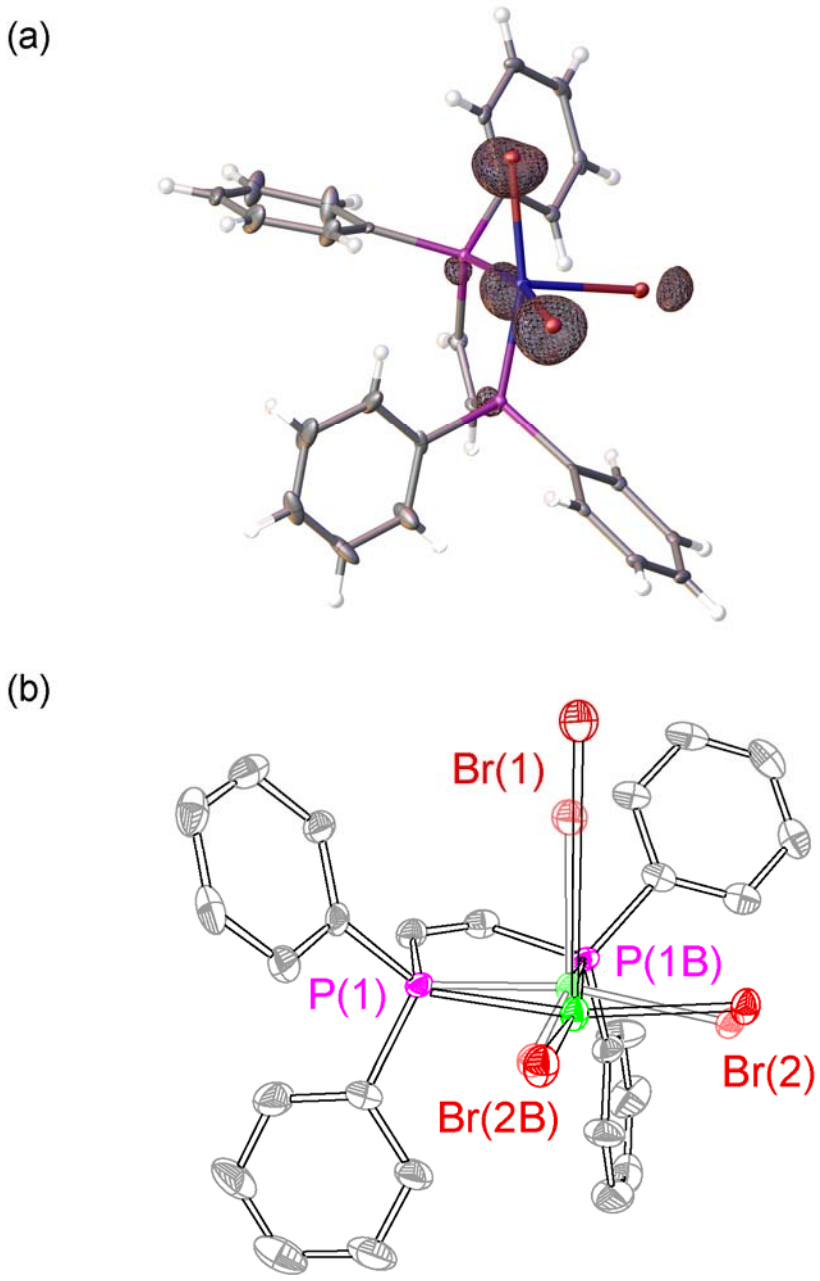

Figure S14. (a) Photodifference map obtained for complex **1c** irradiated with a 365 nm LED (5 mW at the crystal) at 15 K. (b) Thermal ellipsoid plot showing the dark structure (faded) and the irradiated structure (bold) generated from **1c**. This plot was generated by normalizing the positions of the P centers in the dark and irradiated structures to focus on the relative motions of the Br ligand. H-atoms and solvent molecules are omitted for clarity. Ellipsoids are drawn at 50% probability.

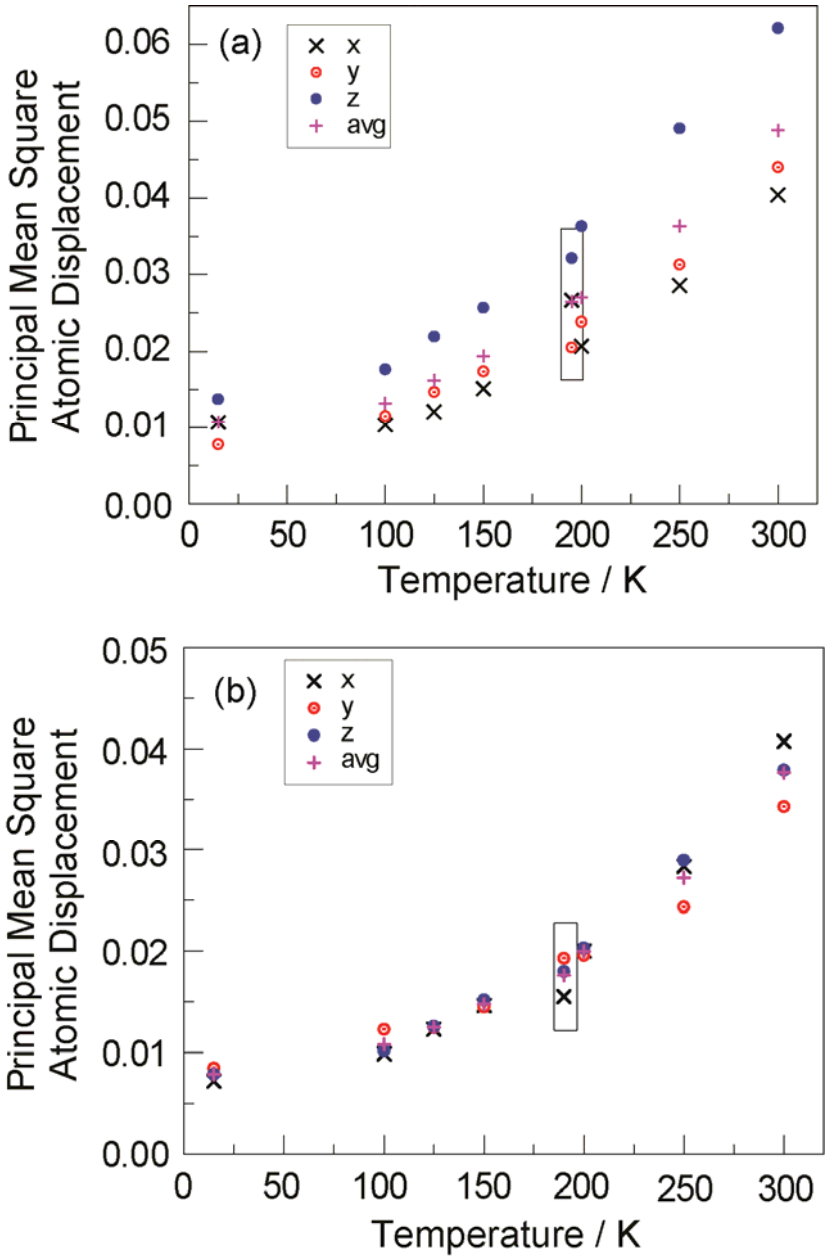

Figure S15. Principal mean square atomic displacements (U) for complex **1c** as a function of temperature plotted for (a) apical bromide atom (b) phosphorous atoms in the ligands. Thermal parameters obtained during photocrystallography are highlighted in a box.

Table S3. Selected metrical parameters for complex **1c** as a function of temperature.

	100 K	125 K	150 K	200 K	250 K	300 K
Ni–Br_{apical} (Å)	2.4312(8)	2.4317(7)	2.4305(7)	2.434(1)	2.428(1)	2.427(1)
Ni–Br_{basal} (Å)	2.3615(6)	2.3595(5)	2.3588(5)	2.3687(9)	2.3605(8)	2.362(1)
Ni–P (Å)	2.224(1)	2.224(1)	2.2245(9)	2.232(1)	2.228(2)	2.231(2)
Ni–Br–Br (°)	96.40(3)	96.38(3)	96.34(3)	96.11(4)	96.10(4)	96.16(5)
P–Ni–P (°)	87.51(6)	87.40(5)	87.35(5)	87.38(6)	87.23(8)	87.15(9)

K. Computational Details

B3LYP calculations were performed using the Gaussian 09. Gas-phase geometry optimizations and frequency calculations for thermochemistry were carried out using an SDD basis set for Ni, P, Cl, and Br and 6-311++G** for all other atoms. The solvation energies were calculated using gas phase optimized geometries with the CPCM solvation model using dichloromethane and acetonitrile as solvents. B3LYP geometries well reproduced experimental metrical parameters, obtained by X-ray crystallography (tabulated in Tables S1 - S3). Time-dependent DFT (TD-DFT) calculations were carried out on a gas-phase optimized geometry of $NiCl_3$(dppe) (B3LYP, TZVP: Ni, P, Br; TZV: C, H) with polarized continuum model (PCM) corrections. The computed absorption spectrum (line broadening 0.25 eV) satisfactorily reproduced the experimental absorption spectrum.

K.1. Energies and XYZ Coordinates

Table S4. Energy of $NiCl_3$(dppe) (**1a**), $NiCl_2$(dppe) (**2a**), and Cl_2 in solvent-corrected energies (Hartree/particle).

	$NiCl_3$(dppe) (**1a**)	$NiCl_2$(dppe) (**2a**)	Cl_2
Thermal Energy, E	–1234.131607	–1219.130347	–29.939352
Thermal Enthalpy, H	–1234.130662	–1219.129403	–29.938408
Thermal Free Energy, G	–1234.230941	–1219.227849	–29.963937

Table S5. Cartesian coordinates of the geometry-optimized $NiCl_3$(dppe) (**1a**).

Atom Type	x	y	z
C	–3.027	–1.16006	–0.57346
C	–3.05043	–2.40778	–1.19988
H	–2.14842	–2.82659	–1.62482
C	–4.24302	–3.12303	–1.25233
H	–4.26697	–4.08829	–1.7434
C	–5.39926	–2.60244	–0.67057
H	–6.32539	–3.16313	–0.71284
C	–5.36407	–1.36309	–0.03215
H	–6.25963	–0.95835	0.423454
C	–4.17661	–0.6388	0.023134
H	–4.14872	0.323072	0.51743
C	–1.92877	1.569298	–0.20034
C	–2.57204	2.283176	–1.21538
H	–2.81532	1.811713	–2.15943
C	–2.91415	3.615819	–1.01025
H	–3.41188	4.167742	–1.79833
C	–2.61468	4.235696	0.202365
H	–2.87241	5.276729	0.355899
C	–1.98541	3.516925	1.215228
H	–1.75089	3.994005	2.158734
C	–1.6455	2.180356	1.020252
H	–1.16828	1.628884	1.817599
C	–0.70358	–0.24039	–2.25697
H	–1.22095	–1.02292	–2.80654
H	–0.95565	0.716234	–2.70837
C	0.801003	–0.48509	–2.24853
H	1.318752	0.078827	–3.02458
H	1.025497	–1.54174	–2.37714
C	1.545216	1.76871	–0.34169
C	1.086857	2.625919	–1.34295
H	0.805227	2.248158	–2.31636
C	0.985339	3.989775	–1.08353
H	0.618019	4.654537	–1.85529
C	1.346568	4.492912	0.164274
H	1.257403	5.553678	0.364894
C	1.812626	3.63341	1.158796
H	2.089013	4.023469	2.130749

C	1.905372	2.267988	0.914379
H	2.235439	1.5919	1.692824
C	3.323362	–0.63948	–0.64356
C	4.371177	0.278812	–0.56168
H	4.170418	1.335542	–0.44605
C	5.684688	–0.17883	–0.63963
H	6.501786	0.529969	–0.58165
C	5.944496	–1.53959	–0.79302
H	6.967667	–1.89119	–0.851
C	4.889646	–2.4505	–0.86877
H	5.0914	–3.50882	–0.9816
C	3.574066	–2.00641	–0.78894
H	2.752735	–2.71106	–0.81758
P	–1.45281	–0.20058	–0.5089
P	1.577719	–0.05834	–0.59669
Ni	0.153924	–0.95812	0.986278
Cl	0.209947	–3.10857	–0.05364
Cl	–1.52343	–1.1885	2.559534
Cl	1.928314	–1.07063	2.462496

Table S6. Cartesian coordinates of the geometry-optimized $NiCl_2$dppe (**2a**).

Atom Type	x	y	z
P	1.531561	–0.0156	–0.39353
Ni	0.00001	–0.00016	1.236194
Cl	–1.68393	0.101547	2.773065
P	–1.53157	0.015514	–0.3935
Cl	1.684001	–0.10212	2.773006
C	–0.66474	–0.36837	–2.03137
H	–0.52748	–1.44875	–2.08191
H	–1.30622	–0.06046	–2.85613
C	2.274547	–1.69156	–0.67369
C	0.664678	0.368184	–2.0314
H	0.527399	1.448563	–2.08195
H	1.306138	0.060267	–2.85616
C	2.899388	1.222634	–0.25119
C	–1.95661	2.736319	0.194828
H	–1.31685	2.554877	1.0485
C	–2.27432	1.691582	–0.67364
C	–2.89963	–1.22248	–0.25123
C	4.230192	0.83752	–0.10016
H	4.499062	–0.21066	–0.08787
C	3.621852	–3.19099	–1.99995
H	4.268727	–3.36458	–2.85151
C	–3.10566	1.918117	–1.77414
H	–3.35585	1.111556	–2.45273
C	3.105904	–1.91796	–1.77419
H	3.356001	–1.11134	–2.45276
C	2.548879	2.575339	–0.24057
H	1.511369	2.876892	–0.32899
C	3.539199	3.543642	–0.10378
H	3.267747	4.592542	–0.09961
C	–2.54937	–2.57525	–0.24084
H	–1.51192	–2.87698	–0.32932
C	–3.62143	3.191227	–1.99985
H	–4.26827	3.364948	–2.8514
C	2.474478	–4.0096	–0.03784
H	2.226473	–4.8206	0.636384
C	5.217113	1.81235	0.039819
H	6.252197	1.513249	0.154298

C	–2.47395	4.009625	–0.03769
H	–2.22586	4.820558	0.636565
C	1.956963	–2.73638	0.194737
H	1.317165	–2.55506	1.048403
C	–4.23036	–0.83714	–0.10004
H	–4.49903	0.211079	–0.08754
C	3.305761	–4.23741	–1.13272
H	3.707295	–5.22776	–1.3117
C	4.874608	3.163276	0.034798
H	5.644124	3.918241	0.143557
C	–3.3052	4.237574	–1.13258
H	–3.7066	5.22799	–1.31152
C	–5.21744	–1.81182	0.039808
H	–6.25247	–1.51255	0.154406
C	–4.87519	–3.16281	0.03451
H	–5.64485	–3.91765	0.143134
C	–3.53986	–3.5434	–0.10418
H	–3.26859	–4.59235	–0.10019

Table S7. Cartesian coordinates of the geometry-optimized Cl_2.

Atom Type	x	y	z
Cl	0.288562	0.049541	–4.441142
Cl	–0.975222	–0.998892	–5.901788

Table S8. Summary of thermochemistry of $NiCl_3$dppe (**1a**) and $NiCl_2$dppe (**2a**).

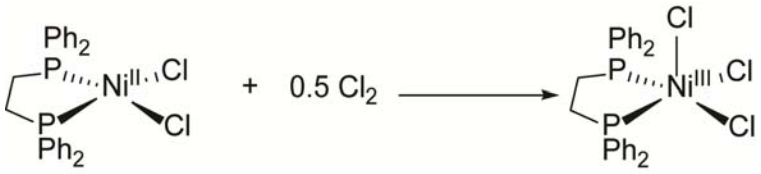

X = Cl	Experimental	DFT (B3LYP)
ΔH (kcal/mol)	–23.7	–20.1
ΔG (kcal/mol)	–	–13.3
ΔS(cal/mol K)	–	–23.0

Table S9. Spin densities, population analyses (β-LUMO), Mayer bond orders.[a]

Complex	Ni(d)[b]	Cl_{ap}(p)[b]	Ni[c]	Cl_{ap}[c]	MBO (α/β)
$NiCl_3$(dppe) (**1a**)	65.51	14.78	0.88	0.17	0.633/0.419

[a] All gas-phase values. [b] Values for the β-LUMO (i.e., the unoccupied d_{z^2} orbital). [c] Mulliken spin density.

K.2. Time-Dependent DFT (TD-DFT) Analysis

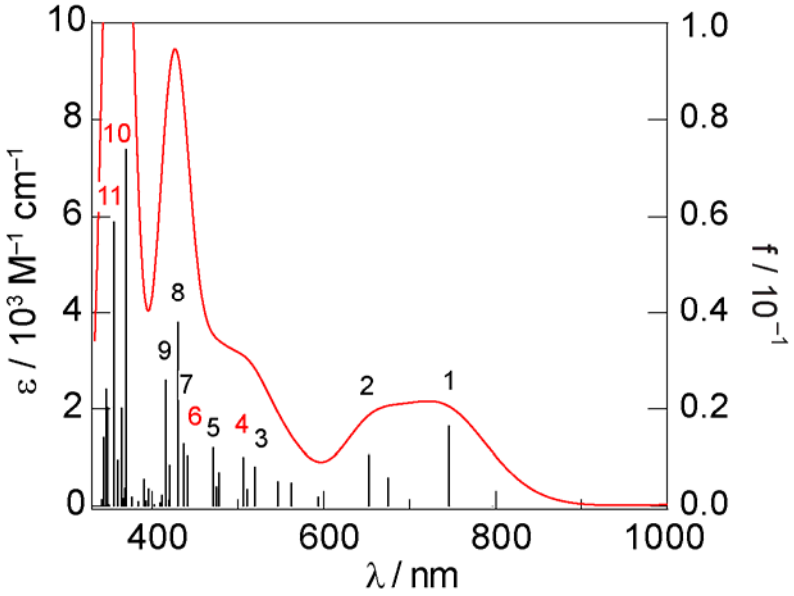

Figure S16. Relevant oscillators (oscillator strength > 0.01; solid black bars) from TD–DFT calculations for complex **1a** with simulated absorption spectrum overlaid (solid red line). Excitations 4 and 6 are predominantly $Cl(p(\pi) \rightarrow Ni(3d_{z^2})$.

Table S10. TD-DFT calculated transitions for $NiCl_3$dppe (**1a**) (PCM = CH_2Cl_2).[a]

State [b]	Energy (nm)	Energy (cm^{-1})	*f* [c]	Contributions	Assignment [d]
1(4)	746	13 400	0.0166	145A → 146A (65%) 143B → 146B (10%)	α(pσ(ap)) → α($d_{x^2-y^2}$)
2(6)	652	15 300	0.0106	142A → 146A (21%) 143B → 146B (17%) 145A → 146A (13 %)	α(pπ(ap)) → α($d_{x^2-y^2}$) + β(pπ(ap)) → β($d_{x^2-y^2}$)
3(12)	506	19 800	0.0101	140A → 146A (17%) 144B → 145B (9%)	α(Phπ) → α($d_{x^2-y^2}$) + β(pπ(ap)) → β($d_{x^2-y^2}$)
4(15)	**471**	**21 200**	**0.0121**	**142B → 145B (38%)** **141B → 145B (13%)**	**β(pπ(ap/ba)) → β(d_{z^2})**
5(16)	441	22 700	0.0105	141A → 146A (14%) 143B → 145B (13%)	α(Phπ) → α($d_{x^2-y^2}$)
6(17)	**436**	**22 900**	**0.0129**	**131B → 145B (13%)** **139B → 145B (13%)** **144B → 145B (11%)**	**β(Phπ) → β($d_{x^2-y^2}$) + β(pπ(ap/ba)) → β(d_{z^2})**
7(18)	430	23 300	0.0380	144B → 146B (19%) 138A → 146A (17%) 140A → 146A (13%)	β(pπ(ap/ba)) → β($d_{x^2-y^2}$) + α(Phπ) → α($d_{x^2-y^2}$)
8(21)	415	24 100	0.0260	137A → 146A (38%)	α(Phπ) → α($d_{x^2-y^2}$)
9(30)	370	27 100	0.0739	139B → 146B (19%) 138B → 146B (14%) 131B → 146B (13%)	β(Phπ) → β($d_{x^2-y^2}$) + β(pπ(ba^d)) → β($d_{x^2-y^2}$)
10(33)	**364**	**27 500**	**0.0203**	**138B → 146B (18%)** **136B → 145B (14%)**	**β(Phπ) → β($d_{x^2-y^2}$) + β(Phπ) → β(d_{z^2})**
11(35)	**355**	**28 200**	**0.0590**	**127B → 146B (11%)** **130B → 146B (10%)** **131B → 146B (10%)**	**β(pσ(ap)) → β(d_{z^2}))**

[a] Transitions with some β d_{z^2} acceptor character are in bold. [b] Consecutively numbered excited states; actual state number from TDDFT calculation is given in parentheses. [c] Calculated transitions with energies less than 350 nm and oscillator strengths greater than 0.0100 are listed. [d] ap = apical ligand, ba = basal ligand.

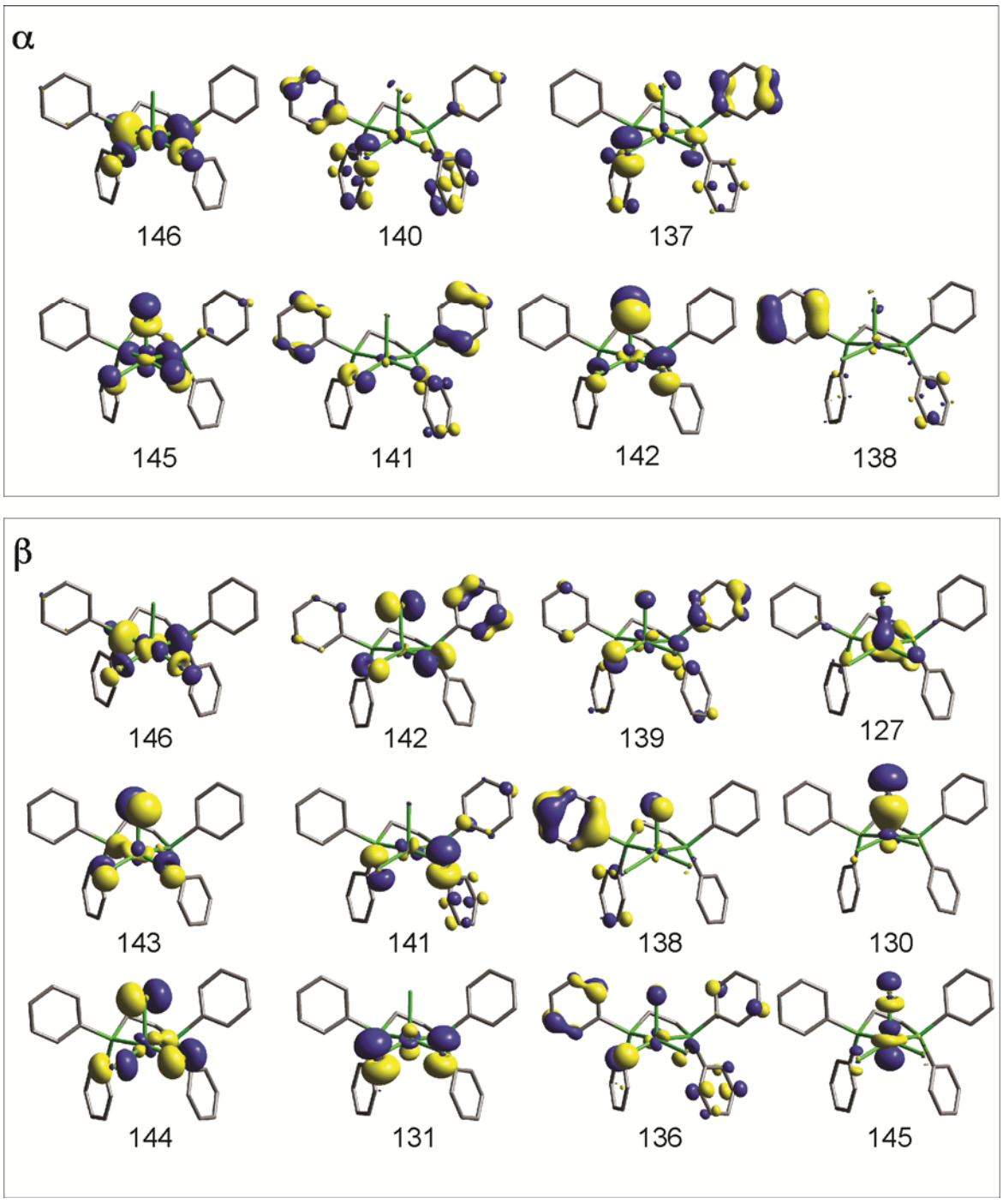

Figure S17. Representative molecular orbitals of complex **1a**.

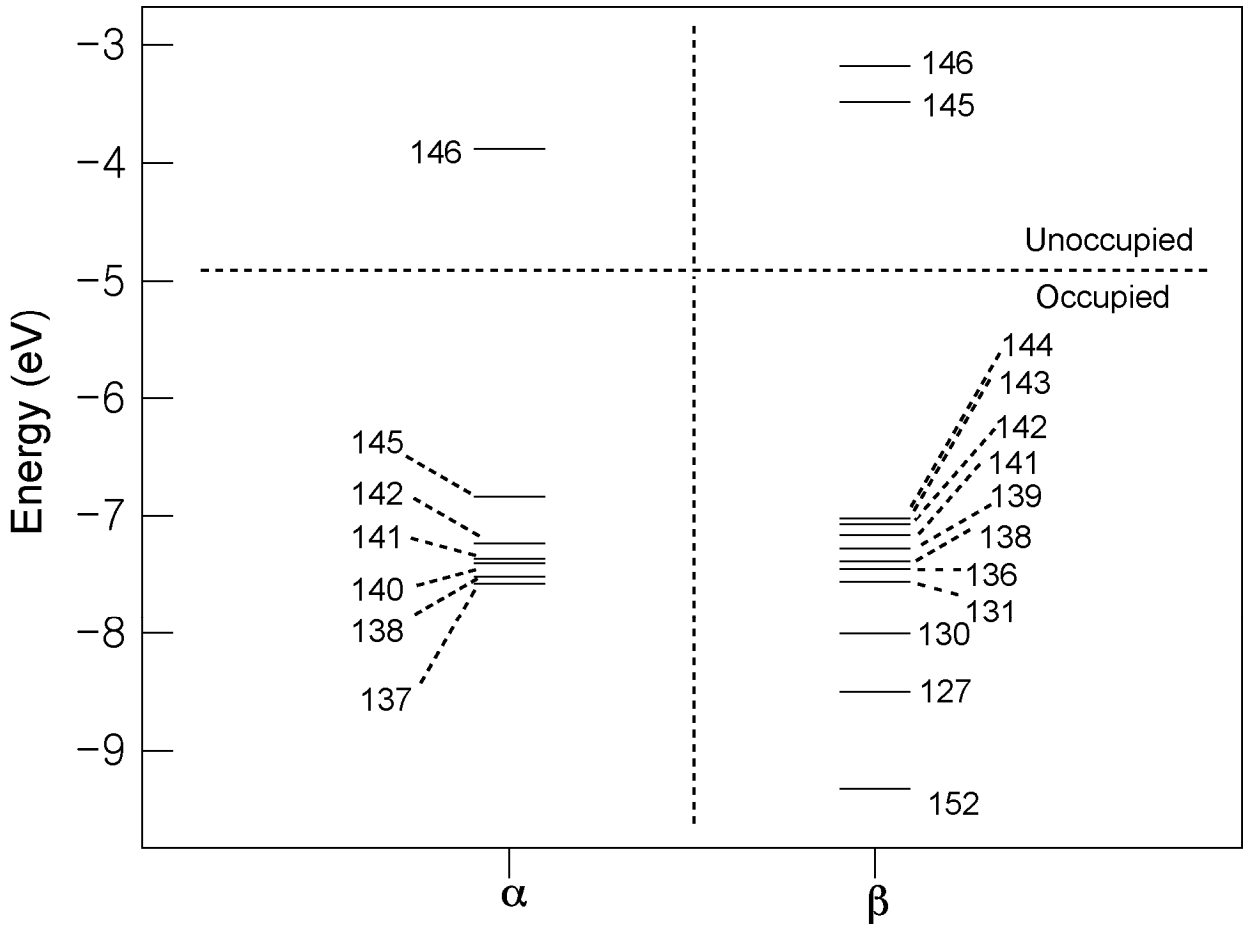

Figure S18. Energy levels of frontier molecular orbitals of complex **1a**.

L. Full Citation for Reference 36

Frisch, M. J.; Trucks, G. W.; Schlegel, H. B.; Scuseria, G. E.; Robb, M. A.; Cheeseman, J. R.; Scalmani, G.; Barone, V.; Mennucci, B.; Petersson, G. A.; Nakatsuji, H.; Caricato, M.; Li, X.; Hratchian, H. P.; Izmaylov, A. F.; Bloino, J.; Zheng, G.; Sonnenberg, J. L.; Hada, M.; Ehara, M.; Toyota, K.; Fukuda, R.; Hasegawa, J.; Ishida, M.; Nakajima, T.; Honda, Y.; Kitao, O.; Nakai, H.; Vreven, T.; Montgomery, J. A., Jr.; Peralta, J. E.; Ogliaro, F.; Bearpark, M.; Heyd, J. J.; Brothers, E.; Kudin, K. N.; Staroverov, V. N.; Keith, T.; Kobayashi, R.; Normand, J.; Raghavachari, K.; Rendell, A.; Burant, J. C.; Iyengar, S. S.; Tomasi, J.; Cossi, M.; Rega, N.; Millam, J. M.; Klene, M.; Knox, J. E.; Cross, J. B.; Bakken, V.; Adamo, C.; Jaramillo, J.; Gomperts, R.; Stratmann, R. E.; Yazyev, O.; Austin, A. J.; Cammi, R.; Pomelli, C.; Ochterski, J. W.; Martin, R. L.; Morokuma, K.; Zakrzewski, V. G.; Voth, G. A.; Salvador, P.; Dannenberg, J. J.; Dapprich, S.; Daniels, A. D.; Farkas, O.; Foresman, J. B.; Ortiz, J. V.; Cioslowski, J.; Fox, D. J. *Gaussian 09*, revision D.01; Gaussian, Inc.: Wallingford, CT, 2009.